Design of a physical point-absorbing WEC model on which multiple control strategies will be tested at large scale in the MASK basin

Conference Paper · January 2015

CITATIONS
3

READS
35

6 authors, including:

Ryan G. Coe
Sandia National Laboratories
69 PUBLICATIONS **327** CITATIONS
SEE PROFILE

Giorgio Bacelli
Sandia National Laboratories
70 PUBLICATIONS **840** CITATIONS
SEE PROFILE

SAND2015-4121C

Design of a Physical Point-Absorbing WEC Model on which Multiple Control Strategies will be Tested at Large Scale in the MASK Basin

Diana L. Bull[1], *Ryan G. Coe*[1], *Mark Monda*[3], *Kevin Dullea*[2], *Giorgio Bacelli*[1], *David Patterson*[1]
[1]Water Power Technologies, [2]Intelligent Systems Control, [3]Robotic and Security Systems
Sandia National Laboratories, Albuquerque, NM 87185-1124

ABSTRACT

A new multi-year effort has been launched by the Department of Energy to validate the extent to which control strategies can increase the power produced by resonant wave energy conversion (WEC) devices. This paper describes the design of a WEC device to be employed by this program in the development and assessment of WEC control strategies. The operational principle of the device was selected to provide a test-bed for control strategies, in which a specific control strategies effectiveness and the parameters on which its effectiveness depends can be empirically determined. Numerical design studies were employed to determine the device geometry, so as to maximize testing opportunities in the Maneuvering and Seakeeping (MASK) Basin at the Naval Surface Warfare Centers David Taylor Model Basin. Details on the physical model including specific components and model fabrication methodologies are presented. Finally the quantities to be measured and the mechanisms of measurement are listed.

KEY WORDS: wave tank; WEC; instrumentation

INTRODUCTION

A large number of theoretical studies (see, e.g., Hals, Falnes & Moan (2011), Babarit & Clement (2006), Scruggs, Lattanzio, Taflanidis & Cassidy (2013)) have shown promising results in the additional energy that can be captured through control of the power conversion chains (PCCs) of resonant WEC devices. The numerical models employed in these studies are, however, idealized to varying degrees. Hence, the project described in this paper comprises both theoretical development as well as experimental validation in order to systematically address the realities confronting real-world devices.

The device type and geometric profile to be studied in the Resilient Nonlinear Controls (RNLC) project was not determined *a priori*. This paper details the rationale employed in determining the device type to be studied and its geometric profile. Each of these aspects is driven by the need to imitate aspects of multiple WEC types while still yielding a system that is highly controllable.

The final geometric profile of the device was tailored to the environment that can be produced in the Maneuvering and Seakeeping (MASK) Basin at the Naval Surface Warfare Centers David Taylor Model Basin. Testing at the MASK basin will occur using a Froude-scale factor of 17; unless otherwise noted, all values in this report are given in model-scale. The selection of the device's design required balancing the physical implications of the model build with the desire to provide the maximum level of flexibility and fidelity in assessment of control strategies. A total of 91 device profiles were studied to select the final device design.

This paper will first present the rationale used to develop the conceptual design of the device to be tested. It will then walk through the methodology employed to determine the physical extent of the device. The specifications of the selected design will then be detailed including the structural implementation and physical properties of the device. The actual performance of the device in the MASK basin will then be shown given the structural implementation and physical properties selected. The paper will conclude with an overview of the on-board instrumentation.

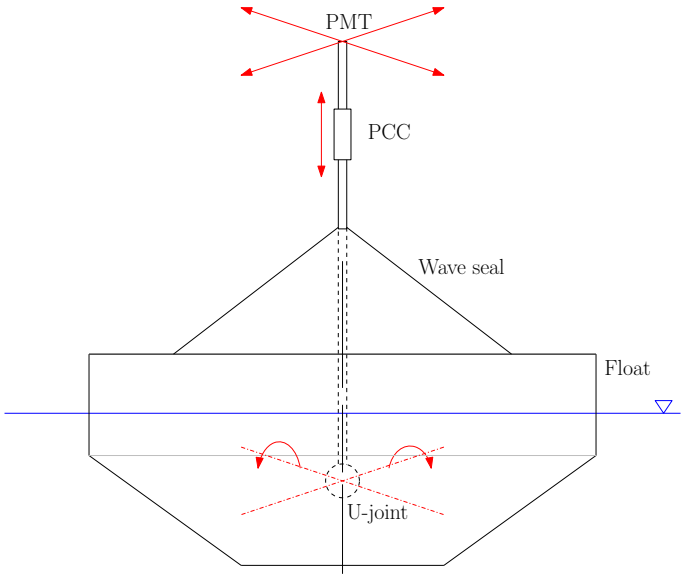

Figure 1: Cartoon of the conceptual T3R2 device design.

CONCEPTUAL DESIGN

The conceptual design of the device to be studied for the next years in the RNLC project was selected after a series of systematic studies and considerations. The WEC was assumed to be a wave activated body operating offshore in 50-150 m of water depth. Further, a point-absorber style was selected so that the device would be small compared to the incident wavelength.

The selection of the device type and geometric profile was aimed at supplying the RNLC project with a test-bed with which to analyze the effectiveness of a range of control strategies in a range of conditions. The design of the WEC needed to imitate many aspects of commercial devices today, however it also needed to be independent and publishable. A cartoon of the conceptual design is shown in Fig. 1 and the sections below will further elaborate on the specific choices shown here. The device's modes of motion, shown by red arrows in Fig. 1, include three translations and two rotations, thus providing a name for the device of the T3R2 - "three-translations, two-rotations."

Device Type

The device type was selected by considering the following design characteristics:

- Location of the device in the water column
- Directional dependencies
- Number of bodies
- Drive-train reference
- Power conversion
- Degrees of freedom (DOFs)
- Mooring and watch circle
- Nonlinearities.

General elaboration on most of these design characteristics and their implications can be found in Bull, Ochs, Laird, Boren & Jepsen (2013), Bull & Ochs (2013b,a).

A surface-piercing device was selected since this is the most energetic portion of the water column. An axisymmetric device was selected for two primary reasons: most devices with directional dependence are designed to weather-vane into the predominant wave direction and the device will be tested in short-crested environments requiring directionality to be considered. A single body was selected to better bound the power conversion requirements. By selecting a single body, this program will not be able to experimentally address control questions regarding multiple wave activated bodies mutually reacting (bodies responding with similar orders of magnitude) to the environment.

Since a single body device was selected, the drive-train must react against an earth-fixed "ground." As the RNLC project is focused on the control of the power conversion chain, it was determined that locating ground above the still water line would provide valuable advantages in reliability. This decision allows for easier access to the power conversion mechanism and additionally obfuscates the need for water-proofing. Given a single body reacting against ground, the power conversion mechanism was selected to work in a single translational (vertical) DOF (see "PCC" in Fig. 1).

The device, however, is selectively allowed to move in three dimensions. The T3R2's float is connected to the power conversion mechanism through a lockable universal joint (see "U-joint" in Fig. 1). The motions of the body in roll and pitch (yaw is not allowed) nonlinearly couple into the heave DOF (Coe & Bull, 2014) thus affecting power conversion. A planar motion table (PMT) allowing the entire device (body plus power conversion mechanism) to translate in the horizontal plane was selected to emulate the mooring systems of most deep water devices (see "PMT" in Fig. 1). The PMT is also selectively controllable such that the device can be locked in a given x-y location. The restoring force provided by the PMT will mimic a compliant mooring system and will result in large natural resonances in surge and sway that are outside of the model-scale waves.

To better approach the reality of ocean-deployed WECs, a number of sources of nonlinearity were intentionally included in the T3R2's design. Additionally, the device was designed such that the presence of these nonlinearities, which include dynamics, viscous losses, overtopping and breaching events, nonlinear hydrostatics/hydrodynamics as well as motion constraints, can be largely controlled, either via mechanical "locks" or through the input to the system (i.e. basin waves). When evaluating surface-piercing commercial WECs, it is clear that most of the nonlinearities influential in the dynamics of industry devices are captured by the T3R2.

Float Geometric Profile

The geometric profile of the T3R2's float (i.e. the cross-sectional shape of the float as depicted in Fig. 1) was selected by considering the following design characteristics:

- Size
- Resonance location
- Structural aspects (center of gravity and buoyancy (COG and COB), moments of inertia (MOI))
- Variable wetted surface profile
- Rate of change of the wetted surface profile
- Overtopping and breaching
- Nonlinear hydrostatics/hydrodynamics
- Viscous damping.

The physical size of the body is important in determining structural/PCC loads and the natural resonances of the device. The device was designed such that the MASK wavemaker can produce waves both below and above the heave resonance. This is important, as it is expected that controls will work distinctly within these two regimes. Further, the heave natural resonance location will set the compatibility to the wave climate. Hence the selection of the size and resonance locations is an iterative process that balances the physical implications for the bearing systems and PCC with the desire for good natural ("uncontrolled") performance in a typical US deployment climate. The COG, COB, and rigid-body MOI were selected to ensure static and dynamic stability. Further they are selected such that the roll and pitch natural resonances are physically separated from the heave natural resonance.

In a single geometric profile, multiple sub-profiles were determined as important in order to increase the applicability of the results to many developers. Further, these sub-profiles allow for nonlinear Froude-Krylov and radiation effects to be selectively prominent. Three distinct aspects can be seen in Fig. 1:

- A horizontal deck, which increases the effect of overtopping on device dynamics
- A vertical wall, in which truly linear responses can be obtained

- A truncated cone section, in which a predictable rate of change of the profile is achieved

The incorporation of sub-profiles in the T3R2 allows for many of the nonlinearities seen in industry devices to be expressed. One nonlinearity that is not strongly highlighted in this design are viscous losses. There will be viscous losses, but they are not expected to be dominant.

An initial parametric shape study was completed on 6 fundamental shapes with varying radii and drafts (Bacelli, Bull & Coe, 2015). A total of 54 device profiles were studied. For each of the shapes, higher-order panels representing the three-dimensional wetted surface were used to model the submerged geometry in a BEM potential flow solver (WAMIT, 2012). Utilizing the shapes' planes of symmetry ($x = 0$ and $y = 0$), one quarter of each shape was modeled. For each of the shapes, the excitation and radiation hydrodynamic coefficients (both in the frequency domain (FD) and in the time domain (TD)) were compared as functions of parameters that characterize each geometry.

This study highlighted the superior radiation properties of the cone in relation to the other shapes. However, in order to allow for systematic testing stages to occur in mostly linear conditions, the project required that the wetted profile around the equilibrium free surface offered a constant water plane area (i.e. a vertical wall). These considerations led to the selection of a truncated cone as the basic shape of the device.

For the selected truncated cone design, more in depth analysis was completed to determine the devices performance in the MASK basin. A total of 37 devices were studied by varying the following aspect ratios

- Ratio of the top radius to the total draft
- Ratio of the top radius to the bottom radius
- Ratio of the draft to the vertical wall draft.

In addition to the hydrodynamic analysis a FD model (Coe & Bull, 2014), which incorporated the T3R2's dynamics with the hydrostatic/hydrodynamic parameters determined via WAMIT, was used to predict performance of the device within the MASK basin.

DETERMINATION OF PHYSICAL DESIGN

Design decisions were driven by one of two reasons: (1) maximization of control strategy testing functionality and (2) constraints imposed by the limits of the MASK basin or structural fabrication. Hence, the final selection of the device profile considered the physical requirements that were imposed on the model build (e.g., bearing reaction forces, maximum linear generator force, and overall size) as well as its predicted performance in the MASK basin.

As stated above, both nonlinear time-domain (TD) (Coe & Bull, 2014, 2015) and linear frequency-domain (FD) models (Coe & Bull, 2014) have been developed to for the RNLC project. Using the FD model, response amplitude operators (RAOs) were obtained for:

- Inertial position, velocity, and acceleration in all five active DOF's,
- Relative position of the waterline on the float (discussed in detail within this section),
- Power conversion force requirements,
- Absorbed power.

These RAO's were obtained for a range of resistive loading values ($0 \leq R_{load} \leq 20\ \frac{\text{kNs}}{\text{m}}$). Data for every R_{load} with a resolution of $0.02\ \frac{\text{kNs}}{\text{m}}$ is saved in these simulations.

In order to ensure that structural requirements were physically realizable, the performance of the device was catered to the capabilities of the MASK basin. By multiplying the largest amplitude that can be produced in the tank by the largest RAO response, the physical model will inadvertently be designed to a larger than necessary factor of safety since the largest amplitude does not necessarily occur at the peak RAO frequency. Wave-maker curves (wave amplitude versus angular frequency) specify the maximum operating envelope and can be used to achieve this catered analysis by multiplying the RAOs by the specific MASK wave-maker curve.

The results of this analysis, presented in a subsequent section, allowed for the quantitative comparions of the 37 truncated cone designs. This comparsion included the following considerations: bearing reaction forces, maximum linear generator force, relative postion of the water line on the float (i.e. variable hydrostatics/hydrodynamics), maximum excursions, and overall size.

Relative Waterline RAO

A series of analyses were conducted to determine the degree to which the instantaneous waterline will move outside of the cylindrical region (see Fig. 1) of the T3R2's float. These analyses were employed to help determine the degree to which the hydrostatics and hydrodynamics of the float will be nonlinear in a given seastate. This can be accomplished in the frequency domain using monochromatic waves; the phase from the motion RAO, ϕ, can be used to create a sinusoidal time series that captures the appropriate physics for the devices response. In combining the wave and device response, it is possible to track the relative waterline of the wave on the device.

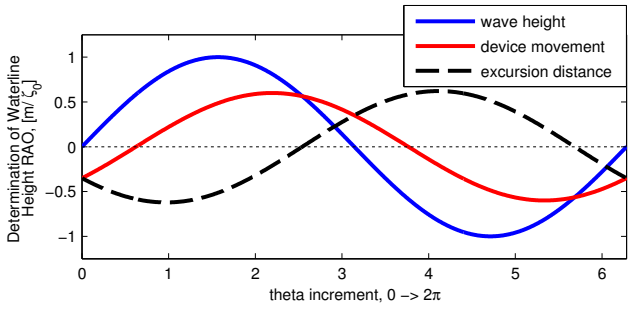

Figure 2: Determination of the maximum waterline excursion over the entire wave cycle for a wave with $\omega = 2.88\ \frac{\text{rad}}{\text{s}}$ when subject to an optimal resistive loading value of $3.6\ \frac{\text{kNs}}{\text{m}}$.

For a wave with amplitude ζ_0 and a frequency of ω, the waveheight, ζ, is given by

$$\zeta(t) = \zeta_0 sin(\omega t). \quad \text{(Eq. 1)}$$

The device motion in response to a wave is given by

$$\eta(t) = \zeta_0 \frac{\eta_0(\omega)}{\zeta_0} sin(\omega t - \phi(\omega)), \quad \text{(Eq. 2)}$$

where the amplitude and phase of the RAO for that frequency are $\eta_0(\omega)$ and $\phi(\omega)$ Thus the instantaneous height of the waves relative to the SWL on the float is given by

$$\eta(t) - \zeta(t) = \zeta_0 \left(\frac{\eta_0(\omega)}{\zeta_0} sin(\omega t - \phi(\omega)) - sin(\omega t) \right). \quad \text{(Eq. 3)}$$

Hence, over an entire cycle $\omega t = 2\pi$, the waterline's largest excursion from the SWL can be found by evaluating Eq. 3 and selecting the maximum. Since the waves are sinusoidal and linear assumptions are used in the creation of the FD model, the relationship between the largest submergence and largest emergence (as measured from the still water line) are symmetrical. An illustration of this procedure can be seen in Fig. 2. Here, the time-domain realization defined in (Eq. 3) is shown for a wave with $\omega = 2.88\,\frac{\text{rad}}{\text{s}}$.

Assessing the maximum of (Eq. 3) at a range of frequencies produces a "waterline position RAO" which can be used in design decisions. In addition to supplying insight into device dynamics, this analysis was also considered in the placement of external sensors (e.g., pressure gauges).

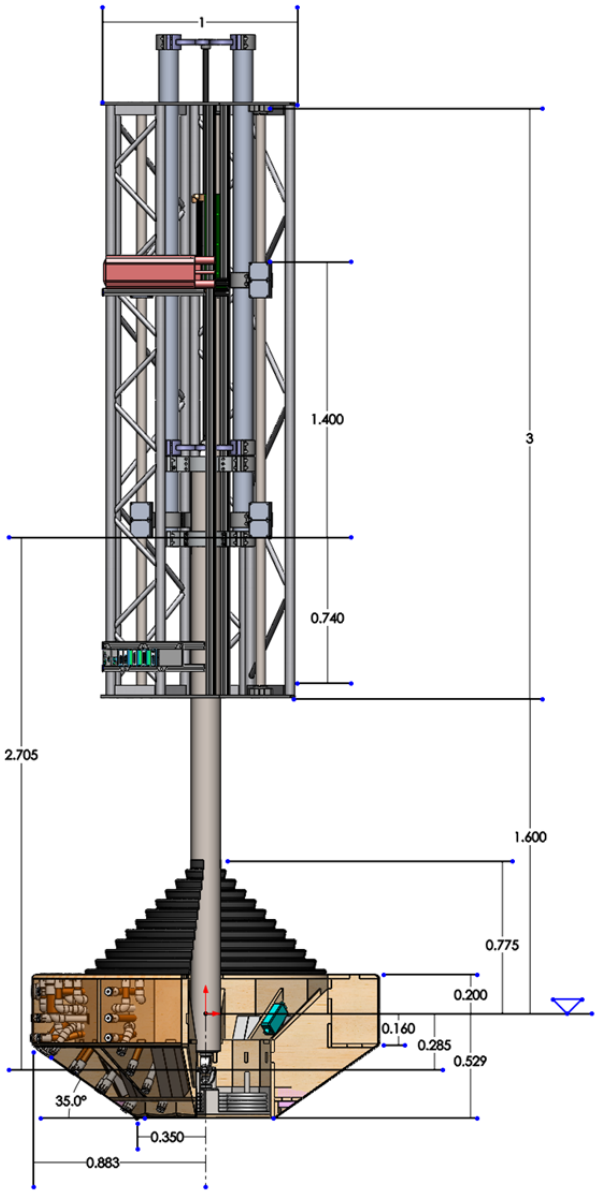

Figure 3: T3R2 geometry and configuration with dimensions in meters.

STRUCTURAL DESIGN

The final device design was selected after implementing the methods detailed in the previous sections. A CAD representation of the selected T3R2 profile is shown in Fig. 3 with the model scale dimensions highlighted. The rigid-body properties of the final design are given in Table 1. Note that the density of water is the fresh water value, not salt water, as the T3R2 is designed entirely around experimental wave tank testing. The COG is the target value used to complete these studies; this value may change slightly as needed for mechanical design. Both the COB and COG locations are reported with respect to the still-water line. Multiple masses are reported to reflect the multi-body nature of this device.

Table 1: Rigid body and general properties of the T3R2.

Property, symbol	**Value**
Fresh water density, ρ	1000 $\frac{\text{kg}}{\text{m}^3}$
Float mass, m_f	644.6 kg
Float MOI, $[I_{xx}, I_{yy}, I_{zz}]$	[84.0 84.0 137.5] kg m^2
Float COG, $[x_{z_G}, y_{z_G}, z_{z_G}]$	[0 0 -0.285] m
Float COB, $[x_B, y_B, z_B]$	[0 0 -0.198] m
Heave mass, m_z	858.4 kg
Heave COG, $[x_{z_G}, y_{z_G}, z_{z_G}]$	[0 0 0.228] m
Surge mass, m_x	1207 kg
Surge COG, $[x_{x_G}, y_{x_G}, z_{x_G}]$	[0 0 1.075] m
Sway mass, m_y	1270 kg
Sway COG, $[x_{y_G}, y_{y_G}, z_{y_G}]$	[0 0 1.103],m
Mooring spring constant, C_m	126.65 $\frac{\text{N}}{\text{m}}$

The natural resonances of this device for each degree of freedom are given in Table 2. The peak hydrodynamic excitation values expected in the MASK basin, which are central drivers to the structural design of the device, are shown in Table 3.

Table 2: T3R2 natural resonance periods.

Degree of freedom	**Natural period (s)**
Surge, x	19.4
Sway, y	19.4
Heave, z	1.66
Roll, ϕ	1.07
Pitch, θ	1.07

Table 3: Largest excitation forces and moments expected in the MASK basin.

Degree of freedom	**Reaction (N, Nm)**
Surge, x	2,878
Sway, y	2,878
Heave, z	7,389
Roll, ϕ	1,757
Pitch, θ	1,757

Bearing Calculations

There are two main bearing assemblies in the physical T3R2 construction. The first allows for vertical travel of the float assembly ensuring the concentricity of the power conversion mechanism. The second set of bearings allow for horizontal travel of the float assembly on the PMT. These bearings must be sized to handle the maximum forces that may be encountered during two operational conditions: PMT unlocked, and PMT locked. In both cases, it is assumed that the float assembly's universal joint is locked, so hydrodynamic moments must also be carried. When the PMT is unlocked, the float and PCC are allowed to accelerate in response to hydrodynamic forces, F_h, on the float. This reduces the magnitude of the forces carried by the vertical bearings. When the PMT is locked, the F_h in surge must be directly balanced by the mooring force, F_m, and higher loads are seen in the vertical bearings.

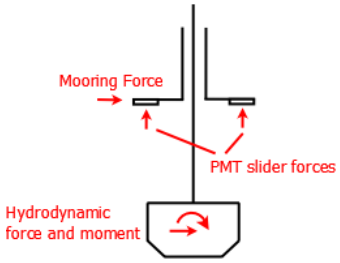

(a) External applied forces, moments, and reactions for the entire moving assembly.

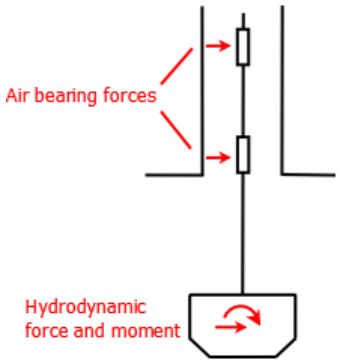

(b) External loads and internal bearing reaction forces on the float subassembly.

Figure 4: Forces used to calculate the loads seen by the vertical PCC air bearings.

Figure 4 shows a simplified 2D schematic with the geometry and forces used to calculate the bearing reaction forces. The calculations are done in 2 parts. First, the forces and moments about the COG of the entire moving assembly are considered. Second, the bearing reaction forces (which are internal forces with respect to the moving assembly) are determined.

Through this process, the forces in the main bearings can be calculated using the hydrodynamic forces and moments, mooring forces, geometry, and mass information. To ensure conservative calculations, the mooring force is assumed to be the spring constant times the maximum possible displacement. Similarly, the maximum hydrodynamic force and moment were assumed to occur simultaneously at maximum PCC extension. These calculations were repeated for all combinations of $\pm F_h$, hydrodynamic moment $\pm M_h$, and $\pm F_m$, and the most conservative case was chosen.

Power Conversion Chain Assembly

The PCC assembly is composed of the tubular linear generator as well as bearing surfaces and a support structure. Fig. 5 shows a CAD model of the PCC assembly.

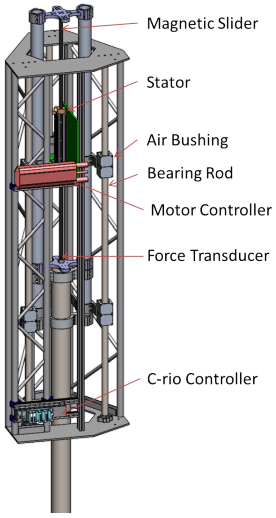

Figure 5: Detailed view of the PCC Assembly.

The LinMot P10-70x400U (LinMot, 2014) was selected as the linear generator of the system based on its stroke length, peak force, response time, and high efficiencies. This device is capable of a peak force of 2700 N with a continuous force of 479 N with air cooling. The stroke length of the design is 1.45 m. A Tritium Wavesculpter200 motor controller has been paired with this PCC (Tritium, 2011).

The T3R2 is designed to accommodate up to four parallel tubular linear generators yielding a total control force of 10,800 N. The peak hydrodynamic excitation in heave is 7245 N and it is not expected that the controller with new control strategies will require more than the excitation force. Further the stroke length is $\sim 3\times$ larger than the expected heave excursion with linear resistive damping applied. This ensures that this physical design can support more demanding control strategies in the future. Motion constraints can be applied virtually, through the motor controller.

In order to minimize frictional losses in the heave direction, air bearings were selected for the PCC arm. Circular New Way air bearings, with tubular bearing surfaces, were selected for their omni-directional load carrying capacity and associated ease of integration (New Way, 2010). Based on a design study, which varied the number and diameter of bearings and bearing rods, solid or tubular rods, and geometry of the device, the configuration shown in Fig. 5 was selected. This system is composed of three 50 mm solid bearing rods in a triangular pattern, with two bearings at each end of each rod, for a total of twelve bearings. The upper and lower bearings are separated by 1.5 m. The 50 mm air bearings are rated at 934 N radial load, so the six lower bearings combined can carry 5604 N. When the U-Joint is locked and the PMT is unlocked the lower bearing force has been calculated to be 3882 N. This results in a safety factor for the air bearing system of 1.44.

While the configuration shown in Fig. 5 is predicted to be within capabilities of the air bearings for normal operation of the T3R2, the special case in which the PMT is locked results in the lower bearing force increasing from 3882 N to 8849 N. Accommodating these loads for the locked PMT condition entirely with air bearings would be quite expensive. Instead, a

Sarraus linkage will be employed when the PMT is locked. This linkage will introduce additional friction to the system though, and thus will be disengaged when not in use.

Planar Motion Table Assembly

The PMT assembly is composed of two main components, an x-y frame designed to allow the entire device to move in translation via two bearing assemblies, and a weldment that connects to the MASK gantry. Fig. 6 shows a CAD model of the PMT assembly.

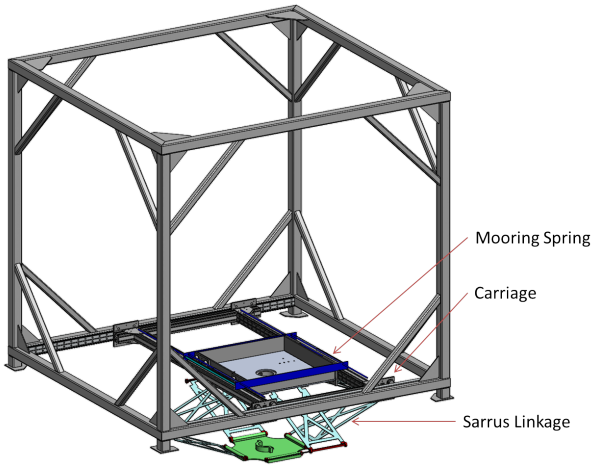

Figure 6: Detailed view of the PMT Assembly.

The mooring restoring force is achieved through the use of custom designed tension springs. The same spring is engaged at opposite ends when traveling in the positive and negative direction through the use of opposing supporting rods. Two springs in parallel are used for each DOF (surge and sway). The device can travel +0.5 m and -1.0 m from its equilibrium position.

The PBC Linear IVT AAQ was chosen to serve as the bearing system for the PMT because its long track length, sufficient load rating, good rolling friction characteristics, easy to integrate form factor, and cheap cost (PBC, 2014). There are a total of eight bearing units (sliders) (four in surge and four in sway). In addition to the reaction forces, each of the four PMT sliders also carry the static weight of the carriage assembly and the vertical LinMot reaction forces. The combined loading that each slider must react against, when the U-Joint is locked and the PMT is unlocked, is 6011 N. Each IVT AAQ bearing surface has a dynamic radial load rating of 10020 N; hence resulting in a safety factor for the PMT bearing system of 1.67. The PMT will be locked by inserting solid steel bars in each translation direction.

Floating Body

Fig. 7 shows a CAD model of the floating body assembly. The floating body will be fabricated from a marine grade plywood frame, closed-cell foam, and coated in fiberglass. Ballast, in the form of lead weights, will be added to obtain the correct total mass and mass distribution. A silicone wave seal will be constructed such that as the floating body rotates with little to no additional restoring force.

The selected universal joint allows for $\pm 45^\circ$ of motion and is a commercial off-the-shelf component designed for a Toyota FJ Crusier. It is rated for 2983 Nm of rotational torque. While it is not intended for axial loading,

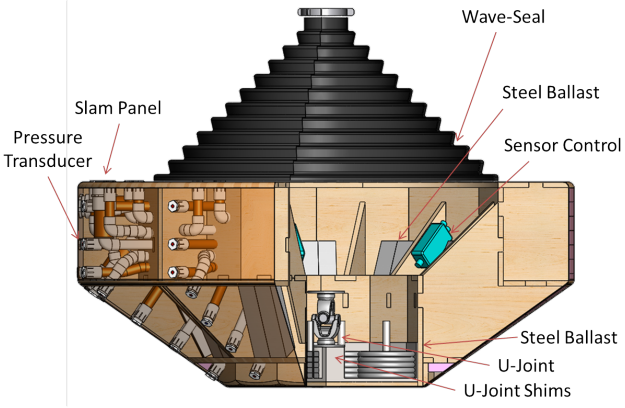

Figure 7: Detailed view of the floating body.

finite element analysis (FEA) results have shown a safety factor of 1.45 in the most extreme case of 10.8 kN being applied on the universal joint from the motors above while the joint is fixed on the bottom. The rotation of the float can be locked via a system in which six tensioned cables run from the top of the float to the connecting arm that runs to the tubular linear generator. Pressure sensors and slam panels (discussed in a subsequent section) will penetrate the float exterior. All instrumentation wires will travel to the data acquisition system within the hollow connecting arm.

PERFORMANCE IN THE MASK BASIN

The optimal R_{load} profile can be solved analytically for regular waves given unlimited PCC force (Falnes, 2002). This is shown by the dashed blue line in Fig. 8. The optimal R_{load} profile given a single PCC is shown in dotted red. The results presented in this section will detail how the final physical design is expected to respond in the MASK basin when optimally controlled with a single PCC (i.e. the dotted red line).

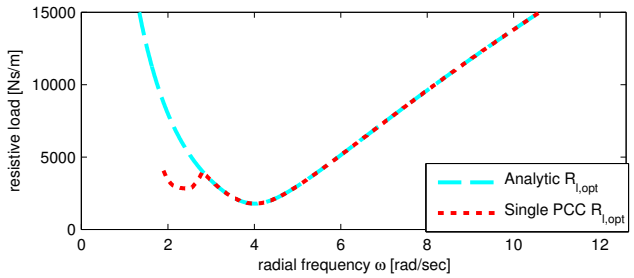

Figure 8: Optimal R_{load} profile for T3R2.

Table 4: Maximum expected values in the MASK basin when one PCC is used to execute the controls.

	Excursion (m, rad)	Velocity ($\frac{\text{m}}{\text{s}}$, $\frac{\text{rad}}{\text{s}}$)	Acceleration ($\frac{\text{m}}{\text{s}^2}$, $\frac{\text{rad}}{\text{s}^2}$)
Surge	0.3906	0.9269	2.3411
Heave	0.4524	1.0621	2.6757
Pitch	0.3020	0.9090	4.0387

The maximum position displacements for the float as a function of frequency are shown in Fig. 9. These are the displacements that are ex-

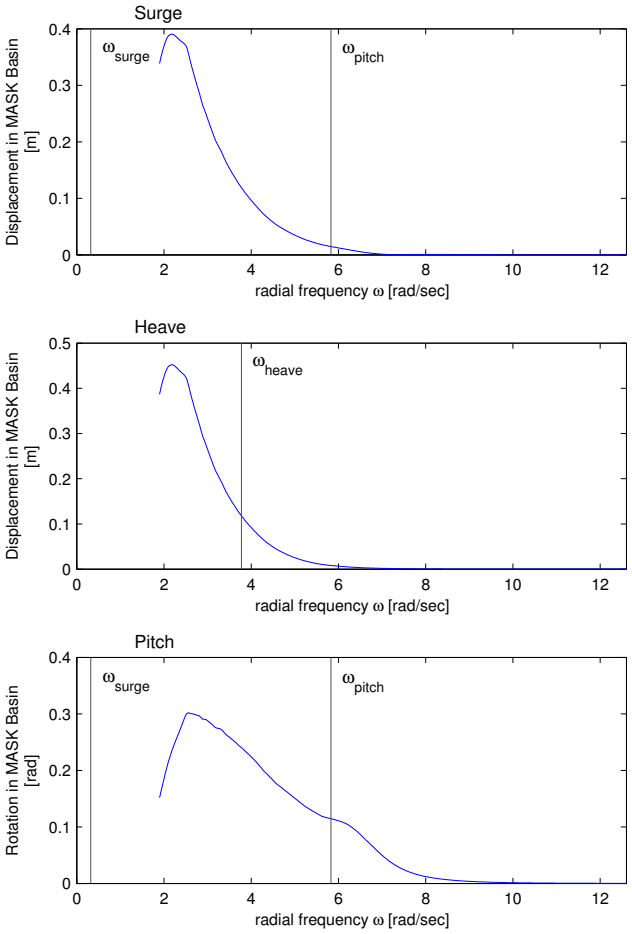

Figure 9: MASK specific motions when subject to optimal PCC resistive loading

pected when operating on the boundary of the wavemaker curve provided by Carderock. The natural resonance locations are shown in Fig. 9. The extrema for this scenario are summarized in Tables 4 and 5.

Table 5: Maximum inertial forces in the MASK basin ($F = ma$) with optimal R_{load} values.

	Reaction (N, Nm)
Surge	2465
Heave	2297
Pitch	255

The waterline height on the float when operating on the boundary of the wavemaker curve is shown in Fig. 10. This figure is presented such that the y-axis indicates the vertical dimension thus serving the dual purpose of communicating the degree of overtopping and breaching as well as marking the float profile to visually enhance the transition points; frequency is shown along the x-axis. The solid colored lines indicate when the waterline has either gone above or below the vertical wall on the float (changes in the profile of the float are indicated with solid lines and corresponding labels). Dotted lines indicate when the waterline will stay within the vertical wall region.

In Fig. 10 it is clear that the waterline will move above and below the

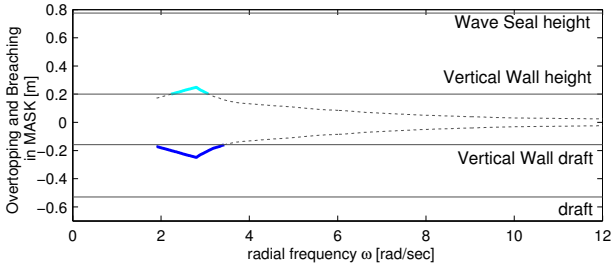

Figure 10: Overtopping and Breaching Heights on T3R2 in the MASK basin. Optimal R_{load} that can be supplied at each frequency given only one PCC.

Table 6: Maximum expected overtoppping and breaching heights on T3R2 given optimal and varying R_{load} values. In the case of the varying R_{load}, the value is choosen to maximize breaching and overtopping.

	Optimal R_{load}	Varying R_{load}
Overtop Depth (mm)	49.2	232.0
Breaching Height (mm)	90.4	273.2

vertical wall region for longer waves in the basin when the optimal control strategy is implemented (when limited to the forcing of a single PCC). Beyond this scenario, the device can also be subject to alternate resistive damping values that will cause larger and smaller degrees of overtopping and breaching. The range between no resistive loading (no controls) and the resistive control strategy that results in the largest waterline excursions shows that control values can be chosen such that the device will stay within the vertical wall region (i.e. mostly-linear hydrostatics) or control values can be chosen in concert with particular wave heights and frequencies that will result in a variable water-plane area. Hence, the device can selectively exhibit the desired nonlinear hydrostatic/hydrodynamic. Table 6 summarizes the extrema given the optimal R_{load} and the R_{load} that causes the maximum overtopping and breaching.

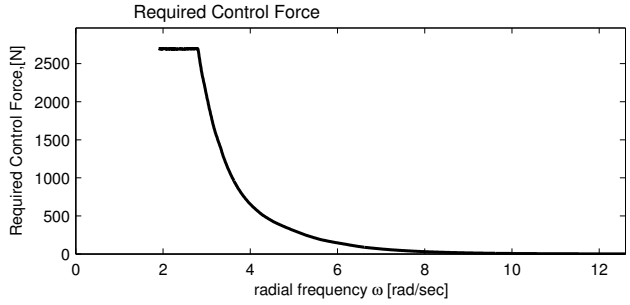

Figure 11: Required force from the PCC to execute the optimal control strategy. Peak value is 2,700 N

The force required from the PCC to execute the optimal resistive loading (shown in red in Fig. 8) is shown in Fig. 11. Clearly, the maximum PCC force of 2700 N is not violated in this case since the resistive loading values were specifically choosen to maintain a maximum of 2700 N.

INSTRUMENTATION

This device has been outfitted with a sensor suite that should be broadly applicable to validate many numerical models: low fidelity (linear flow BEM models (time or frequency), mid-fidelity (non-linear potential flow), and high fidelity (CFD) models. The dynamics of the device in the MASK basin were used to direct the sensor placement on the device and determine magnitude and fidelity requirements. More details on the sensors and data acquisition can be found in Patterson, Bull, Bacelli & Coe (2015).

Translational motions and forces in the surge and sway directions will be measured using string potentiometers (0-1.5 m) and low profile load cells (0-333.6 N). Heave motion will be recorded by the tubular linear generator in the form of differential voltage signals. Heave force will be recorded using a low profile load cell (3336 N). The rotations of the floating body will be recorded by measuring the linear displacement of the body in opposing directions with respect to the PCC connection arm.

Three nontraditional slam panels have been designed to measure high impact short duration events like reentry upon breaching, waves breaking on the device, etc. Due to their nontraditional design, these slam panels are colocated with pressure sensors. Accurate measurement of slam must incorporate the elasticity of the material. These slam panels attempt to mimic the materials elasticity by matching the natural resonance of the structure with a low spring constant spring (22.9 $\frac{\text{kN}}{\text{m}}$) placed in parallel with a very stiff load cell (292 $\frac{\text{kN}}{\text{m}}$, rated to 22.24 N). Additionally, the deflection of the panel will be measured with an linear voltage displacement transducer as an additional corroboration of the measured force.

An array of 27 pressure sensors will be used for multiple purposes: to validate the predicted pressure distribution on the body, to measure the pressure profile of the incident wave, and to corroborate the slam panel measurements. As shown in Fig. 12 these are generally arranged on rays located along 0°, 20°, and 60°; deviations from the rays were required due to physical constraints. The 20 sensors with the primary purpose of measuring the wave-structure interaction pressure have a full-scale accuracy of 0.4% and are rated to 34.5 kPa. The 4 pressure sensors intended to measure the wave pressure fluctuation were selected to minimally achieve a 3.5 mm resolution in wave amplitude while maintaining the same 34.5 kPa range. The 3 slam pressure sensors are encased in oil in order to negate the effects of temperature increases during an impact and have a very fast rise time. These sensors are rated to 103.4 kPa and have a full-scale accuracy of 0.25%.

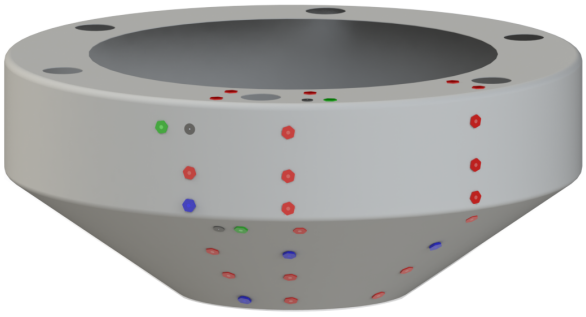

Figure 12: Diagram indicating location and type of pressure sensor and slam panel. Red sensors are the primary sensors with lower accuracy. Blue sensors have higher accuracy with 3mm resolution. Green sensors are the pressure sensors for measuring slam.

Finally, additional state measurements will be made to verify the health of the system. Vibrations will be measured on the PCC assembly and the PMT frame using accelerometers. Humidity and temperature will also be monitored.

CONCLUSIONS

A model-scale WEC device has been designed for use within a research project focused on the development and assessment of advanced WEC control strategies. The physical device will be tested in Carderock's MASK basin using a Froude scale factor of 17.

The rationale employed in determining the device type to be studied and its geometric profile was explained. A methodology developed and employed to determine the physical size of the device that balanced bearing reaction forces, maximum linear generator force, relative postion of the water line on the float (i.e. variable hydrostatics/hydrodynamics), maximum excursions, and overall size. With a fully specified device, the performance model was then used to determine expected motions and forces in order to cater the placement and fidelity of the on-board instrumentation.

The first experiment will occur in the summer of 2015. All results will be made publically available.

ACKNOWLEDGMENTS

This work was funded by the U.S. Department of Energy's Wind and Water Power Technologies Office. Sandia National Laboratories is a multiprogram laboratory managed and operated by Sandia Corporation, a wholly owned subsidiary of Lockheed Martin Corporation, for the U.S. Department of Energy's National Nuclear Security Administration under contract DE-AC04-94AL85000.

REFERENCES

Babarit, A. & Clement, A. (2006). Optimal latching control of a wave energy device in regular and irregular waves. *Applied Ocean Research*, *28*(2), 77–91.

Bacelli, G., Bull, D., & Coe, R. (2015). Resilient nonlinear control: WEC shape study. Technical Report SAND2015-XXXX, Sandia National Laboratories.

Bull, D. & Ochs, M. E. (2013a). Technological cost-reduction pathways for attenuator wave energy converters in the marine hydrokinetic environment. Technical Report SAND2013-7207, Sandia National Laboratories.

Bull, D. & Ochs, M. E. (2013b). Technological cost-reduction pathways for oscillating water column wave energy converters in the marine hydrokinetic environment. Technical Report SAND2013-7205, Sandia National Laboratories.

Bull, D., Ochs, M. E., Laird, D. L., Boren, B., & Jepsen, R. A. (2013). Technological cost-reduction pathways for point absorber wave energy converters in the marine hydrokinetic environment. Technical Report SAND2013-7204, Sandia National Laboratories.

Coe, R. G. & Bull, D. L. (2014). Nonlinear time-domain performance model for a wave energy converter in three dimensions. In *OCEANS*, St. John's, Canada. IEEE.

Coe, R. G. & Bull, D. L. (2015). Sensitivity of a wave energy converter dynamics model to nonlinear hydrostatic models. In *Proceedings of the*

ASME 2015 34th International Conference on Ocean, Offshore and Arctic Engineering (OMAE2015), St. John's, Newfoundland. ASME.

Falnes, J. (2002). *Ocean Waves and Oscillating Systems*. Cambridge; New York: Cambridge University Press.

Hals, J., Falnes, J., & Moan, T. (2011). A comparison of selected strategies for adaptive control of wave energy converters. *Journal of Offshore Mechanics and Arctic Engineering*, *133*(3), 031101.

LinMot (2014). LinMot P10-70-Dxx. http://www.linmot.com/products/linear-motors/p10-70x/.

New Way (2010). New Way Air Bearings. http://www.newwayairbearings.com/products/air-bushings-metric.

Patterson, D., Bull, D., Bacelli, G., & Coe, R. (2015). Instrumentation of a WEC device for controls testing. In *Proceedings of the 3rd Marine Energy Technology Symposium*, Washington DC.

PBC (2014). IVTAAQ linear guides. http://www.pbclinear.com/IVTAAQ.

Scruggs, J. T., Lattanzio, S. M., Taflanidis, A. A., & Cassidy, I. L. (2013). Optimal causal control of a wave energy converter in a random sea. *Applied Ocean Research*, *42*, 1–15.

Tritium (2011). Wavesculptor200 Motor Inverter. http://tritium.com.au/products/wavesculptor200-motor-inverter.

WAMIT (2012). *WAMIT User Manual* (7 ed.). Chestnut Hill, MA.